Optical, stability and energy performance of water-based MXene nanofluids in hybrid PV/thermal solar systems

AS Abdelrazik[1], KH Tan[2], Navid Aslfattahi[3], A. Arifutzzaman[2], R. Saidur[2,4,*], FA Al-Sulaiman[1,5]

[1]Mechanical Engineering Department, King Fahd University of Petroleum & Minerals, Dhahran, Saudi Arabia
[2]Research Center for Nano-Materials and Energy Technology (RCNMET), School of Science and Technology, Sunway University, Bandar Sunway, Petaling Jaya, 47500, Selangor, Darul Ehsan, Malaysia
[3]Department of Mechanical Engineering, Faculty of Engineering, University of Malaya, 50603, Kuala Lumpur
[4]Department of Engineering, Lancaster University, Lancaster, LA1 4YW, UK
[5]Center of Research Excellence in Renewable Energy (CoRERE), King Fahd University of Petroleum & Minerals, Dhahran, Saudi Arabia

*Corresponding author: saidur@sunway.edu.my

Abstract

Solar thermal collectors have been recognized as promising devices for solar energy harvesting. The absorbing properties of the working fluid are crucial because they can significantly influence the efficiency of the solar thermal collectors. The performance of photovoltaic-thermal (PV/T) systems can be optimized by applying nanofluids as working fluids. MXene is a newly developed 2-D nanomaterial that has proven excellent potential in electrical applications with a lack of research in the thermal and optical applications. The present work extensively studied the optical potential of the water/MXene nanofluids with respect to the variation of MXene concentrations (0.0005-0.05 wt. %) and types of surfactant (CTAB or SDBS) used in a hybrid PV/T system. The relationship between the investigated parameters was evaluated through an experimental correlation. The evaluation of the nanofluids in term of the transmittance was conducted through the Rayleigh method. The MXene concentrations and the types of the surfactant play predominant role in the transmittance, absorbance and dispersion stability of the water/MXene nanofluids. The corresponding effects due to these factors become the most noticeable in the wavelengths of 300-1350 nm. Low concentration of the MXene and shorter path lengths lead to higher transmittance. The application of the low concentration of water/MXene nanofluids as the optical filtration in a hybrid PV/T system yields a higher performance compared to a conventional PV/T system. Therefore, this research work provides novelty value in understanding the impacts of using water/MXene nanofluid in the hybrid PV/T solar collectors to harness additional energy.

Keywords: Water/MXene; Nanofluid; Optical filtration; PV/T; Solar energy

Nomenclature

T	temperature, ˚C	E	energy, J
L	length of PV/T system, m	G	solar radiation, W m^{-2}
W	width of PV/T system, m	h	heat transfer coefficient, W m^{-2} K^{-1}
z	height, mm	k	thermal conductivity, W m^{-1} K^{-1}
m	mass, kg	dx	spatial step, m
$\dot{m}$	mass flow rate, kg s^{-1}	dt	time step, sec
c_p	specific heat, J kg^{-1} K^{-1}	v	velocity, m s^{-1}
Greek symbols			
α	absorption coefficient	τ	transmittance
β	temperature coefficient, K^{-1}	ϕ_w	weight fraction
ε	emissivity	η	efficiency
θ	the inclination angle of the system	λ	wavelength
Subscripts			
amb	ambient	*el*	electrical
g	glass cover	*th*	thermal
of	optical fluid	*el, eq*	equivalent electrical
pv	PV module	*bf*	base fluid (water)
cf	cooling fluid	*sky*	sky
bp	back plate	λ	spectral
Abbreviations			
PV/T	photovoltaic/thermal		

1. Introduction

World energy demand has enhanced drastically over the last few decades due to the enormous growth of the globe economy and it is expected to increase by 60% by the year 2030 [1]. The scale of the emission of CO_2 reported for 2018 (33.1G tons) reveals the enormity of the impact and consumption of fossil fuels on environmental issues, including globe climate change, air pollution, ozone layer depletion, and acidic rain [1]. Considering that the energy from the hourly solar flux incident on the Earth's surface is greater than the world energy demand of one year [2], the expectation of the society at large-scale is that the renewable and sustainable energy generation technologies may both fulfill the global energy demand and overcome the detrimental impact on the environment. Approximately 3,400,000 EJ of the solar radiation is estimated to reach the earth in one year, which is 7500 times the world energy demand of one year (450 EJ) [3].

Due to the eco-friendly nature and safety aspects of solar energy as well as the fact that it is an abundant source of energy without a limitation, almost 70% of world energy demand is expected to be supplied by solar energy technologies by 2100 [4]. Solar thermal and photovoltaic (PV) technologies are the two main approaches used for solar energy harvesting [5]. Solar PV technologies are capable of

direct conversion of the sunlight to electricity, while solar thermal systems use the harvested solar energy to heat water, air or other fluids. According to the global installed capacity of the solar energy (about 70%), solar thermal systems are more popular compared to PV technologies. The thermal collector, which handles the photo-thermal conversion of solar spectrum, is the critical component of a solar thermal system [6]. Solar thermal collectors can be categorized into three classes based on the operating temperature: i) collectors with low-temperature operation such as flat-plate and evacuated-tube collectors, ii) collectors with medium-temperature operation such as parabolic troughs, and iii) collectors with high-temperature operation, comprising of power towers and dish-concentrators [7]. The above classification is based on the temperature of the working fluid into the thermal collectors. For instance, the flat-plate type thermal collectors can achieve fluid temperatures up to ~100 °C. The main challenge of producing an effective thermal collector is selecting a suitable absorber and a working fluid for efficient conversion of the incident solar radiation into thermal energy [8]. Using the appropriate working fluid can potentially optimize the efficiency of the thermal collectors.

Nanofluids have provided outstanding improvements in terms of optical and thermo-physical properties over traditional HTFs. Mu et al. [9] have demonstrated experimentally that a noticeable amount of the visible light is transmitted through the water/SiO_2 nanofluid, and the TiO_2 and ZrC nanofluids absorb most of the solar spectrum (ZrC has the highest absorbance). Sani et al. [10] have reported that 100% of solar energy was absorbed by water/single-walled carbon nanotubes at a loading of 0.05 g/L and a penetration path of 1 cm. Mercatelli et al. [11] evaluated the extinction coefficient of the water/single-walled carbon nanotubes at a fixed wavelength of 632.8 nm, and found that it varies linearly with the concentration of single-walled carbon nanotubes. Taylor et al. [12] conducted a comprehensive research on the amount of solar radiation absorbed by different types of water-based nanofluids containing graphite, copper, silver, aluminum, and gold nanoparticles. They have reported absorbance values higher than 95% for all the studied nanofluids at a 10-cm collector depth. The extinction coefficient is a measure of the light absorbing strength of a substance at a particular wavelength. Taylor et al. [12] have theoretically investigated the improvement of the extinction coefficient. They compared the measured extinction coefficient of the studied nanofluids with the values obtained using Maxwell-Garnett and Rayleigh scattering approximation models. They concluded that the Maxwell-Garnett model gives better prediction of the results at longer wavelengths when compared with short wavelengths (visible range). Said et al. [13] evaluated the impacts of concentration and/or size of TiO_2 nanoparticles on the extinction coefficient through Rayleigh approach. They have reported that the smaller particle size (less than 20 nm) has negligible impact on the optical properties of the nanofluids and the relationship between the volume fraction and extinction coefficient is linear. Tyagi et al. [14] reported that the solar radiation absorbance of water/aluminum nanofluid is nine times that of pure water. According to them, as the absorbance and transport of solar energy can be targeted simultaneously in a volumetric absorption collector, nanofluids can enhance the energy efficiency and

lessen the energy loss. Jing et al. [15] studied the optical and thermal properties of silica/water nanofluid at different nanoparticles sizes. The authors reported that for a nanoparticles size of 5 nm and a volume fraction of 2%, the transmittance of the nanofluid was up to 97%, which is nearly the transmittance of a pure water. However, the thermal conductivity was higher by 20% for the water/silica nanofluid. Using CFD simulation to apply their results on a PV/T system, they have found that water/silica at size of 5 nm and volume fraction of 2% is the best for a PV/T system.

Lee et al. [16] adopted a Mont Carlo algorithm combined with the Mie scattering theory to assess the optical properties of the nanofluids. Taylor et al. [17] designed optical filters using nanofluids with suspended core/shell nanoparticles for PV/T systems. They achieved higher efficiency of solar energy harvesting compared to that of conventional optical filters. Recently introduced two-dimensional materials (called MXene family), which are comprised of early transition metal carbides/nitrides, represent supreme thermo-physical properties [18]. Chemical etching is conducted on the materials so-called $M_{n+1}AX_n$ phases to selectively remove the A layers, where A is mostly adopted from group IIIA/IVA of the periodic table, M represents a transition metal, X indicates C or N and n is denoted as 1, 2, or 3. The resulted MXene and its composites exhibit a promising feature of electromagnetic radiation absorption capability, which is contributed by their high electromagnetic interface (EMI) shielding effect in nature, as reported by Shahzad et al. [19]. Their finding has driven the great efforts given by the other scientists in studying the relationship between the MXene and certain electromagnetic waves, such as the sunlight. Excellent radiation absorption and the subsequent heat generation done by these materials could possibly render them to become the supreme material for light-to-heat (photo-thermal) conversion.

Several attempts have been made to assess the optical performance of the nanofluids [11–15]. The unique applicability of the nanofluids in the hybrid PV/T solar collectors is mainly due to their ability of transmitting solar radiation, demanding the comprehensive research that is related to the optical characterization on these materials. The transmittance of nanofluids is very important optical parameter to determine their utility for optical filtration. The principle of using filtration device in the PV panels is to selectively transmit the solar radiation in its beneficial range. Consequently, the efficiency of a hybrid PV/T system strongly depends on the transmittance of optical filter. Meanwhile, the dispersibility of the nanofluids are also closely related to their light transmittance capability. The developed nanofluids in current study, represent promising dispersibility performance based on the zeta potential measurement values. The preparation of a good dispersion of the water-based MXene nanofluids is the most challenging part. Surfactants could be used to achieve homogeneous water/MXene nanofluids. Hence, in this study, two different surfactants, sodium dodecyl benzene sulphonate (SDBS) and cetyltrimethylammonium bromide (CTAB) were used separately to prepare water/MXene nanofluids for the application in a hybrid PV/T system. The prepared nanofluids work as the optical filters of solar radiation. Zeta potential measurement, Fourier transform infrared (FTIR) spectroscopy, UV-Vis

spectroscopy, and morphology determination were conducted to determine the suitability of the as prepared nanofluids for applications in hybrid PV/T systems. After the characterization of the water/MXene nanofluids they were incorporated into a hybrid PV/T system.

The novelty of the current study is the development of promising water/MXene nanofluids using two different types of surfactants as a new optical filter with high stability for enhancement of optical performance in a hybrid PV/T system. For the analytic evaluation of the developed nanofluids, a modified Rayleigh method was used in solar thermal applications. A new correlation between the viscosity and stability of the as-prepared water/MXene nanofluids was developed. The transmittance spectra of the water/MXene nanofluids proved that the type of surfactants can influence the transmittance spectra effectively. The water/MXene nanofluid prepared using the SDBS surfactant displays higher spectral transmittances when compared to that prepared using the CTAB surfactant. For both surfactants, an inverse relationship was observed between the MXene nanoflakes concentration and the transmittance spectra of the prepared water/MXene samples. The influence of the nanoflakes concentration on the transmittance spectra was significant. The effect of the surfactant and the nanoparticles-concentration was most observed in the range of 300 – 1350 nm, which corresponds to the Ultraviolet (UV), the Visual (Vis) and the Near Infrared (NIR) ranges. Also, the as prepared water/MXene nanofluids have a good extinction coefficient of ~1.5 $Lg^{-1}cm^{-1}$, revealing sufficient light absorption capability even at a low concentration of MXene in the nanofluids. The experimentally acquired results indicate that absorbance is directly proportional to the concentration of MXene nanoflakes. To the best of authors' knowledge, there are a very limited number of experimental studies undertaken to investigate the band gap of MXenes. In this study, the band gap energy of the nanofluids with the highest concentration of 0.05 wt. % MXenes dispersed using CTAB or SDBS are determined using the Tauc method employing the Kubelka-Munk function. For the water/MXene nanofluid with a low concentration of 0.0005 wt. %, the efficiency of the hybrid PV/T system is about 20%. Thus, the findings of the present study reveal that optical filtration using the water/MXene nanofluid at a low concentration in a hybrid PV/T system can provide a superior performance compared to the standalone PV system.

2. Methodology

The water/MXene nanofluid as optical filtration for hybrid PV/T systems was evaluated experimentally. The impact of the concentration of the nanoparticles and the type of surfactant on the optical properties and stability of the nanofluid were investigated. After preparation of the water/MXene nanofluids, the characterization and the optical properties were determined as a function of the nanoparticles concentration. Finally, the electrical and thermal performance of a hybrid PV/T system using the emerging MXene-based nanofluids were investigated.

2.1 Materials and preparation

Sodium dodecyl benzene sulfonate (SDBS) was procured from Sigma Aldrich as a surfactant in the ionic self-assembly reaction of cyclophene BIMCP-1. Cetyltrimethylammonium bromide (CTAB) was supplied by Sisco Research Laboratories Pvt. Ltd. with a molecular weight of 364.45 and a shelf life of 60 months.

2.1.1 Synthesis of delaminated MXene flakes (d-Ti_3C_2)

In the synthesis of MXene (Ti_3C_2) the following materials were used without any further purification: MAX phase material (Ti_3AlC_2), lithium fluoride (325 mesh powder, 98.5% purity, Alfa Aesar), hydrochloric acid (37% w/w, 12 M, Fisher chemicals), and sodium hydroxide (97% purity, pellets, Sigma Aldrich). First, 30 ml of HCl (6M) solution was prepared by diluting 15 ml of the concentrated HCl with 15 ml of the DI water in a 50 ml beaker. Then 3 g of LiF was poured to the HCl solution, followed by stirring at 300 rpm for 30 minutes until dissolved. This etching process was continued by adding 3 g of MAX phase material (Ti_3AlC_2) to the solution slowly (within 15 minutes) to avoid overheating (exothermic reaction), and the resultant solution was stirred at 40 °C for 48 h. After the etching process, a dilute solution of NaOH was added slowly until the pH of the solution reached 6, and the solution was filtered, and the solid product rinsed several times with DI water. The product was washed further 4 times (each time of 10 minutes) at 3500 rpm using an ultrahigh speed centrifuge (Sorvall LYNX 6000, thermo scientific). The sonication process (1 h) for the produced multilayered MXene (m-Ti_3C_2) was conducted by using an ultrasonic probe sonicator (FS-1200N) to obtain delaminated flakes of MXene. The synthesized delaminated flakes of MXene nanomaterial were dried in a vacuum oven (VO 500, MEMMERT Germany) overnight.

2.1.2 Preparation of water/MXene (Ti_3C_2) nanofluids

Water/MXene (Ti_3C_2) nanofluids were prepared at five different concentrations, consisting of 0.0005, 0.001, 0.005, 0.01, and 0.05 wt. % by using two different surfactants. 3 mg of each of CTAB and SDBS surfactants were used for the preparation of the samples. To prepare the 0.0005 wt. % water/Ti_3C_2 nanofluid, 0.75 mg of Ti_3C_2 and 3 mg CTAB were added to 150 ml of DI water in a 300 ml beaker and the resulting mixture was stirred at 600 rpm for 30 minutes to obtain a homogenous dispersion. The dispersion was sonicated using an ultrasonic probe sonicator (FS-1200N) for 1 h at a power of 70% and an on/off time of 7/3 sec. The same protocol was used to prepare the 0.0005 wt. % water/Ti_3C_2 nanofluid with the SDBS surfactant. The water/Ti_3C_2 nanofluids at other concentrations of 0.001, 0.005, 0.01, and 0.05 wt. % were prepared using the same procedure with 1.5, 7.5, 15, and 75 mg of Ti_3C_2, respectively.

2.2 Characterization of the stability and optical properties

2.2.1 Determination of the stability of the water/MXene (Ti_3C_2) nanofluids

The surfactants CTAB and the SDBS are used in the preparation of the water/MXene nanofluids to achieve adequate dispersion of MXene in water. To ensure that stable dispersions are formed, the stability of the prepared nanofluids with different concentrations of the nanoparticles was determined. The stability of the prepared nanofluids were determined through three different methods; (i) zeta potential measurements, (ii) visual inspection, and (iii) transmittance monitoring. The zeta potential was measured immediately after preparation of the nanofluids to evaluate the dispersion quality, while the other two methods were used to monitor the changes in stability with time. These three methods are described in the following sections.

Zeta Potential Measurement

The main aim of the zeta potential measurement is to obtain information on the surface charge of a material. Litesizer 500 Anton Paar was used for the determination of the stability of the prepared water/Ti_3C_2 nanofluids. This equipment measures the stability based on the concept of electrophoretic light scattering (ELS). The control temperature of the Litesizer 500 is in the range of 0-90 °C. The light source of this equipment is a laser with a power of 40 mW and wavelength of 658 nm. Zeta potential measuring range is from -600 to +600 mV, with a sensitivity of 1 mg/mL (lysozyme) and maximum sample concentration of 40% w/v.

Visual Inspection

Visual inspection is the simplest method available to assess the changes of nanofluids with time. The prepared nanofluid samples were filled in the clear glass vials and were allowed to stand undisturbed for 7 days. Photographs of the vials with their contents were taken at regular intervals during the 7 days. Using the variation of the appearance, the stability of the nanofluids was assessed.

Monitoring of Transmittance to Assess the Degradation of Nanofluids

Monitoring the transmittance of a sample is a novel method proposed in this study to assess the stability of a nanofluid. In this method the transmittance of a nanofluid is measured at different times after preparation to determine its stability. The rate of sedimentation of nanoparticles in a nanofluid determines its lifetime, and thus, its stability. As sedimentation will affect the transmittance of the nanofluid, monitoring the change of the transmittance of the nanofluid with time can be used to determine its stability.

The transmittance spectra of the prepared nanofluids were determined by using a UV-Vis

spectrometer, for 7 days after preparation and the results were used to determine the rate of change of transmittance with time, which indicates the stability of a nanofluid.

2.2.2 Morphology and microstructure analysis of water/MXene (Ti_3C_2) nanofluids

The synthesized MXene (Ti_3C_2) was characterized using FESEM (Hitachi SU8010). Dispersion and homogeneity of the prepared nanofluids was also checked using scanning electronic microscopy (VEGA3, TESCAN) and energy-dispersive x-ray spectroscopy (EDX, OXFORD INSTRUMENT). A digital ion coater (COXEM Co, SPT-20) was used to coat the samples with Pt at a fixed current of 3 mA for 300 seconds for SEM imaging.

2.2.3 Fourier transform infrared spectroscopy

Perkin Elmer Spectrum Two-UATR spectroscope with an integrated detector of MIR TGS (15000-370 cm^{-1}) was used to obtain the FTIR spectra and detect the peaks due to water and water/Ti_3C_2 nanofluids. The scanning speed used to detect the FTIR spectra of the water and the nanofluids is 0.2 cm/s with an optimum scan range of 4000-1000 cm^{-1}.

2.2.4 UV-Vis spectroscopic characterization of water/MXene (Ti_3C_2)

Perkin Elmer Lambda 750 spectroscope was used to conduct ultraviolet-visible (UV-Vis) absorption for all the prepared nanofluids. The absorption spectra were collected in the wavelength ranged from 200 to 2500 nm at room temperature. The adjusted scan speed (266.75 nm/min) with the incident wave of 860 nm monochromatic is applied.

UV-Vis spectroscopy was conducted to examine the optical behavior of the prepared water/MXene nanofluids by using two different surfactants (CTAB in 0.36 mM and SDBS in 0.38 mM). UV-Vis absorption of the nanofluids containing MXenes at concentrations of 0.0005 wt. %, 0.001 wt. %, 0.005 wt. %, 0.01 wt. %, and 0.05 wt. % were determined using a 1 cm thickness quartz cuvette at a fixed wavelength (Figure 13).

If the Beer-Lambert Law is followed, there is a directly proportional relationship between the concentration and the absorbance of a sample [20,21]. Therefore, based on the basis of Eq. 1, the molar absorptivity, ε_A can be calculated as shown in Eq. 2, which is determined by the resulted line gradient of A against lc [21].

$$A = \varepsilon_A lc \quad \text{Eq. 1}$$

Where:

A is absorbance intensity of a sample

ε_A is molar absorptivity/extinction coefficient ($M^{-1}cm^{-1}$)

l is path length of light (cm)

c is concentration of absorbing species (M)

By rearranging Eq. 1, the ε_A can be represented in Eq. 2.

$$\varepsilon_A = \frac{A}{lc} \quad \text{Eq. 2}$$

Another optical parameter, namely optical absorption coefficient (α) is calculated by using Eq. 3, which is resulted by combining both Eq. 4 and Eq. 5. It measures the fraction of light absorbed per unit length of a medium that can show how well the studied MXenes can absorbs light [22,23].

$$\alpha = (\ln 10\, A)/l \quad \text{Eq. 3}$$

$$A = -\log_{10} T_r \quad \text{Eq. 4}$$

$$\alpha = \frac{1}{l}\ln\frac{1}{T_r} \quad \text{Eq. 5}$$

Where, α is absorption coefficient (cm^{-1}) and T_r is the transmittance intensity of a sample.

The band gap energy of the sample with the highest concentration of MXenes was determined using the most widely used method proposed by Tauc et al. [24]. The so-called the Kubelka-Munk function is applied and is presented in Eq. 6 [25,26]. The band gap energy is deduced from the intercept of extrapolated linear part of the Tauc plot of $(\alpha E)^2$ versus photon energy (E).

$$\alpha E = \alpha_o (E - E_G)^n \quad \text{Eq. 6}$$

where:

E is photon energy which is converted from the interacted wavelengths (eV)

E_g is the band gap energy corresponding to transitions indicated by the value of n (eV)

α_o is a constant which depends on the transition probability

n is a value which can be 1/2, 3/2, 2 or 3 depending on types of electronic transition

2.3 Performance of hybrid photovoltaic/thermal (PV/T) system under influence of nanofluids

An evaluation is presented to study the influence of both the MXene nanoflakes loading and the types of surfactant toward the operation efficiency of a PV/T solar system. The water/MXene nanofluid acts as the optical filtration. The assessment of the operation is based on the evaluation of the average PV temperature, in addition to the thermal and electrical efficiencies of the hybrid PV/T system with optical filtration. The hybrid system consists of an optical filtration channel that is directly attached to the front surface of a PV panel. Another cooling channel, with water as flowing fluid, is attached at the bottom

of the PV panel to provide the cooling from the backside of the panel. The height of the optical filtration channel is 1 cm, which equals to the cuvette size (optical path length) used through the measurements of the transmittance spectra of the prepared water/MXene nanofluids. The evaluation parameters were calculated at three concentrations of the MXene nanoparticles, in the range from 0.0005 wt. % to 0.05 wt. %. The efficiencies were calculated for a whole-day study in mid-July (15th of July) in Dhahran, Saudi Arabia. The experimentally determined spectral transmittance was used to assess the performance. A comparison was held between the assessment parameters, as mentioned earlier, for both the current hybrid system and a conventional PV/T system with a single cooling channel at the bottom side of the panel. The relevant differential energy equations were developed and solved numerically by using Finite Difference Method in Matlab 2017b software. The aforementioned studied system is illustrated in Figure 1.

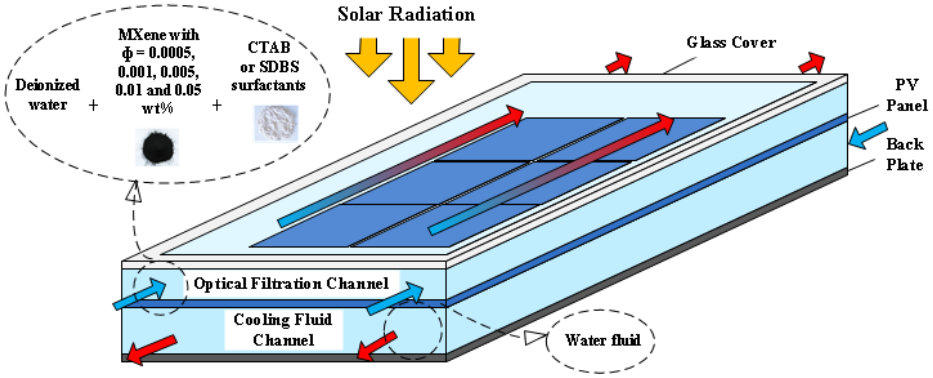

Figure 1. Schematic diagram of the hybrid PV/T system with the water/MXene nanofluid acts as the optical filtration.

2.3.1 Mathematical model

As mentioned, the assessment of the performance of the hybrid PV/T system was implemented using its thermal and electrical outputs. Table 1 and Table 2 list the developed energy equations and the fixed parameters, respectively.

Table 1. Energy equations of the hybrid PV/T system with the water/MXene nanofluids as the optical filtration.

Components	Equations	Numbering System
Glass cover	$z_g\rho_g cp_g\frac{\partial T_g}{\partial t}=\alpha_g\int_{0.25\mu m}^{2.5\mu m}G_\lambda d\lambda+h_{rad,g}(T_{sky}-T_g)+h_{conv,g}(T_{amb}-T_g)+h_{conv,of}(T_{of}-T_g)+\frac{1}{dx}\int_{-x}^{+x}t_g k_g\frac{\partial T_g}{\partial x}$	Eq. 7
Optical fluid	$z_{of}u_{of}\rho_{of}cp_{of}\frac{\partial T_{of}}{\partial x}=\tau_g\int_{0.25\mu m}^{2.5\mu m}\alpha_{of,\lambda}G_\lambda d\lambda+h_{conv,of}(T_g-T_{of})+h_{conv,of}(T_{pv}-T_{of})$	Eq. 8
PV panel	$z_{pv}\rho_{pv}cp_{pv}\frac{\partial T_{pv}}{\partial t}=\tau_g\left\{\alpha_{pv}\int_{0.25\mu m}^{2.5\mu m}\tau_{of,\lambda}G_\lambda d\lambda-[1-\beta_{pv}(T_{pv}-T_{ref})]\int_{0.25\mu m}^{2.5\mu m}\tau_{of,\lambda}\eta_{ref,\lambda}G_\lambda d\lambda\right\}+h_{conv,of}(T_{of}-T_{pv})+h_{conv,cf}(T_{cf}-T_{pv})+\frac{1}{dx}\int_{-x}^{+x}t_{pv}k_{pv}\frac{\partial T_{pv}}{\partial x}$	Eq. 9
Cooling fluid	$z_{cf}u_{cf}\rho_{cf}cp_{cf}\frac{\partial T_{cf}}{\partial x}=h_{conv,cf}(T_{pv}-T_{cf})+h_{conv,cf}(T_{bp}-T_{cf})$	Eq. 10

Back plate	$z_{bp}\rho_{bp}cp_{bp}\frac{\partial T_{bp}}{\partial t} = h_{conv,cf}(T_{cf} - T_{bp}) + h_{rad,bp}(T_{ground} - T_{bp}) + h_{conv,bp}(T_{amb} - T_{bp}) + \frac{1}{dx}\int_{-x}^{+x} t_{bp}k_{bp}\frac{\partial T_{bp}}{\partial x}$	Eq. 11

The electrical and thermal efficiencies are calculated by using Eq. 12 and Eq. 13:

$$\eta_{elec} = \frac{E_{el}}{E_{in}} \quad \text{Eq. 12}$$

$$\eta_{th} = \frac{E_{th}}{E_{in}} \quad \text{Eq. 13}$$

where notations E_{in}, E_{el} and E_{th} represent the solar input, electrical output and thermal output energies, respectively and they are calculated using Eq. 14, Eq. 15 and Eq. 16.

$$E_{in} = LW\int_0^{\Delta T_{study}}\left[\int_{0.25\mu m}^{2.5\mu m} G_\lambda d\lambda\right]dt \quad \text{Eq. 14}$$

$$E_{el} = LW\int_0^{\Delta T_{study}}\left[\tau_g\int_{0.25\mu m}^{2.5\mu m}\tau_{of,\lambda}G_\lambda\eta_{c,ref,\lambda}\left[1-\beta\left(T_{pv}-T_{ref}\right)\right]d\lambda\right]dt \quad \text{Eq. 15}$$

$$E_{th} = LW\int_0^{\Delta T_{study}} \dot{m_{of}}\, c_{p,of}\left(T_{of,out} - T_{of,in}\right)dt \quad \text{Eq. 16}$$

Where, LW represents the front surface area of the PV panel.

Figure 2 shows the weather data at the mid-July (15th of July) [27], while Figure 3 depicts, both, the spectral distribution of the incident solar radiation defined by ASTM G-173 [28] and the reference efficiency of the PV panel provided by Jing et al. [15] for the monocrystalline silicon PV cells.

In order to provide a fair comparison between the current PV/T system and the conventional standalone PV system, the equivalent electrical efficiency is calculated. The equivalent electrical efficiency combines both the normal electrical efficiency and the electrically-equivalent thermal efficiency of the system. By assuming of a conversion efficiency (thermal energy to electrical energy) of 40%, which generally represents the normal conversion efficiency in gas and combined power stations [29], the equivalent electrical efficiency is given by Eq. 17:

$$\eta_{elec,eq} = \eta_{elec} + 0.4\,\eta_{th} \quad \text{Eq.17}$$

Table 2. Fixed parameters in the study

Parameter	Value	Parameter	Value
L	0.7 m	ε_g	0.9
W	0.3 m	τ_g	0.9
z_g	3 mm	α_g	0.05
z_{of}	10 mm	α_{pv}	0.945
z_{pv}	3 mm	ε_{bp}	0.09
z_{cf}	20 mm	T_{ref}	25˚C
z_{bp}	3 mm	ΔT_{study}	1 day = 86400 sec
Δx	0.05 m	$\dot{m}_{of}$	0.001 kg/s

v	0 m s^{-1}	**$\dot{m}_{cf}$**	0.002 kg/s

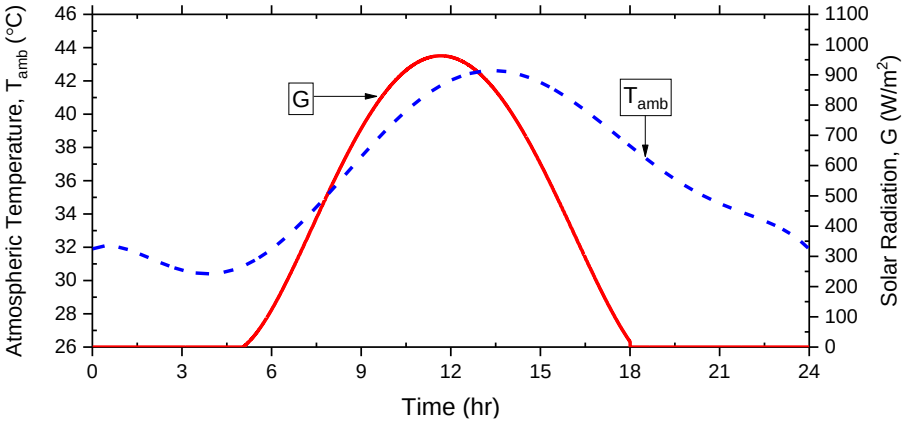

Figure 2 Weather data at the mid-July in Dhahran, Saudi Arabia [27]

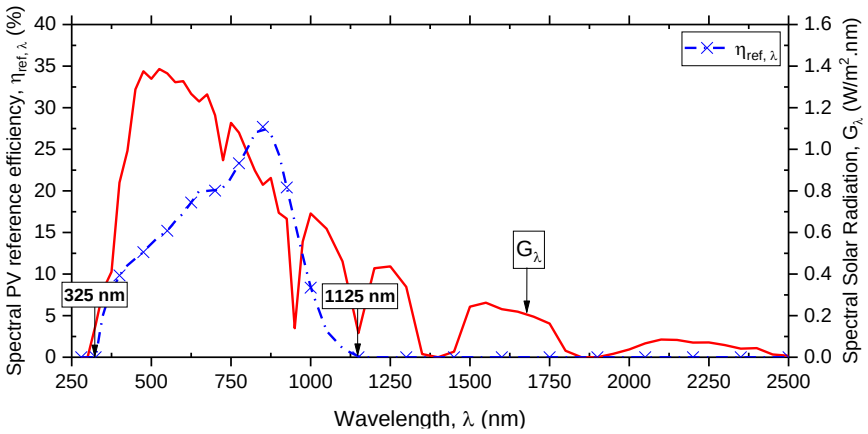

Figure 3 The spectral distribution data used in the study for the PV reference efficiency [15] **and for the solar incident radiation** [28]

3. Results and discussion

3.1 Stability characterization of the nanofluids

3.1.1 Zeta potential

Immediately, after the preparation of the water/MXene nanofluids, the dispersion quality of the MXene nanoparticles in water was assessed by the determination of the average zeta potential for each sample. An average absolute value of the zeta potential of over 30 indicates the presence of a good dispersion and a highly stable nanofluid. The higher the average absolute value of zeta potential, the higher the stability of the dispersion of the nanofluid. Table 3 demonstrates the measured average zeta potential for each of the prepared samples and the results indicate that all samples possess good dispersion of nanoparticles resulting in stable nanofluids. In addition, the surfactant SDBS produces more stable dispersions, especially at the

lower concentrations of 0.0005 wt. %, 0.001 wt. %, and 0.005 wt. %, which is confirmed by visual inspection and the transmittance measurement methods.

Table 3. Average zeta potential values for the samples of the water/MXene nanofluid prepared at different concentrations using CTAB and SDBS surfactants.

Concentration of nanoparticles, ϕ (wt. %)	Zeta potential of water/MXene nanofluids	
	CTAB surfactant	SDBS surfactant
0.0005	55.59	-124.71
0.001	60.34	-71.59
0.005	62.64	-64.70
0.01	56.63	-55.11
0.05	58.01	-55.98

3.1.2 Visual observation

Figure 4 and Figure 5 show the results of the stability assessment by using visual observation of the water/MXene nanofluid samples prepared with CTAB and SDBS surfactants, respectively. The visual observation was conducted for 7 days at regular intervals. The results for the water/MXene samples prepared with CTAB shown in Figure 4, indicate that sedimentation of the nanoparticles increases with time. A majority of the nanoparticles in the low concentration samples (0.0005 wt. % and 0.001 wt. %) settle down in 3 hours, while the nanofluids of a higher concentration remain largely intact. After 1 day, almost all the nanoparticles in the three nanofluids with lower concentrations settle down and at 5 days all the nanoparticles settle to the bottom. Most of the nanoparticles into two nanofluids with a higher concentration have also settled down.

After preparation

After 1 hour

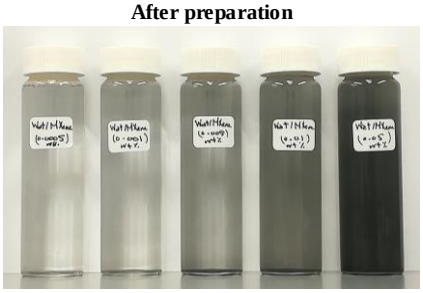

After 3 hours

After 6 hours

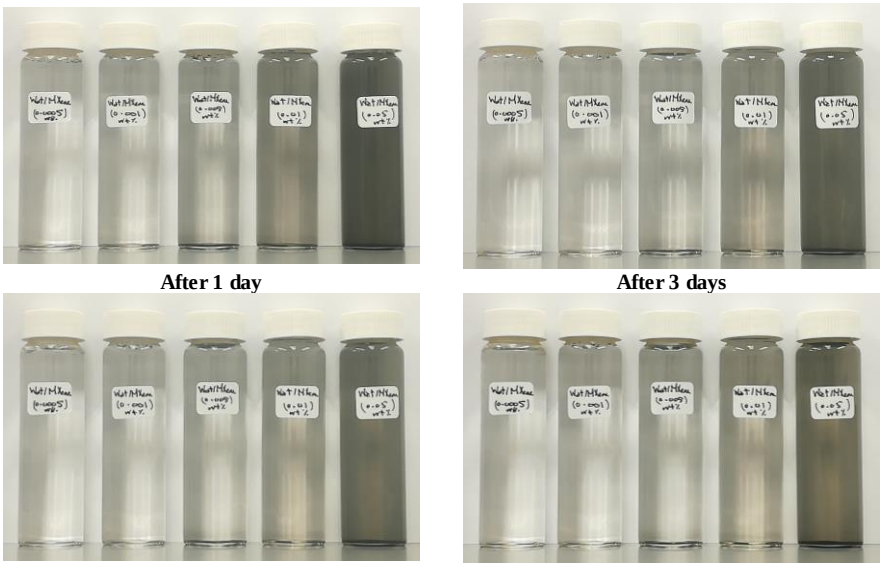

Figure 4 Visual observation to determine the stability of water/MXene samples prepared with the CTAB surfactant during 7 days after preparation.

As shown in Figure 5, the water/MXene samples prepared with SDBS surfactant display a similar behavior. Some of the samples were not able to maintain their stability even for few hours after preparation. After 5 days, most of the nanoparticles in the nanofluids of all concentrations settle to the bottom.

The effects of the CTAB and the SDBS surfactants on the stability of the water/MXene nanofluid samples cannot be determined using visual observation due to the differences in their measured transmittance immediately after preparation, which is attributed to the effect of the surfactants themselves. However, the most stable nanofluid can be found using daily measurements of the transmittance to determine the degradation of the nanofluids.

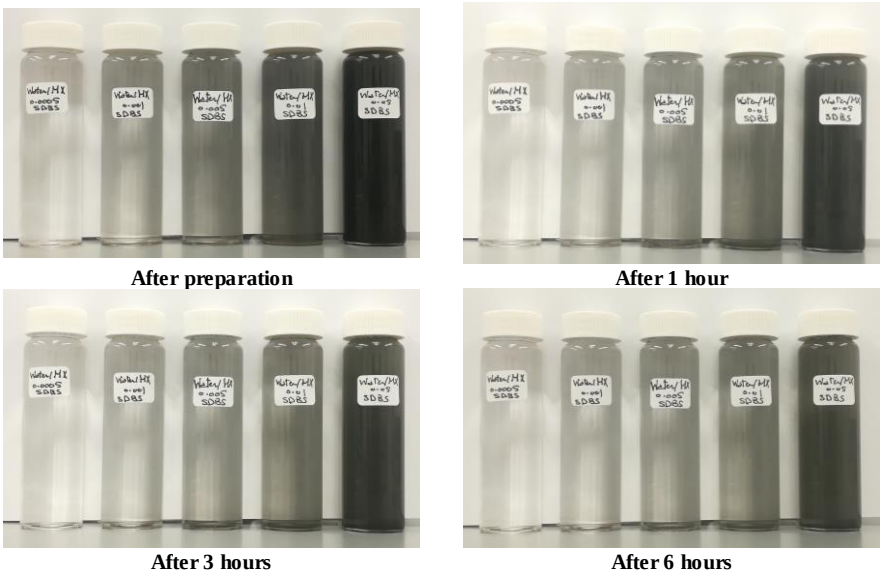

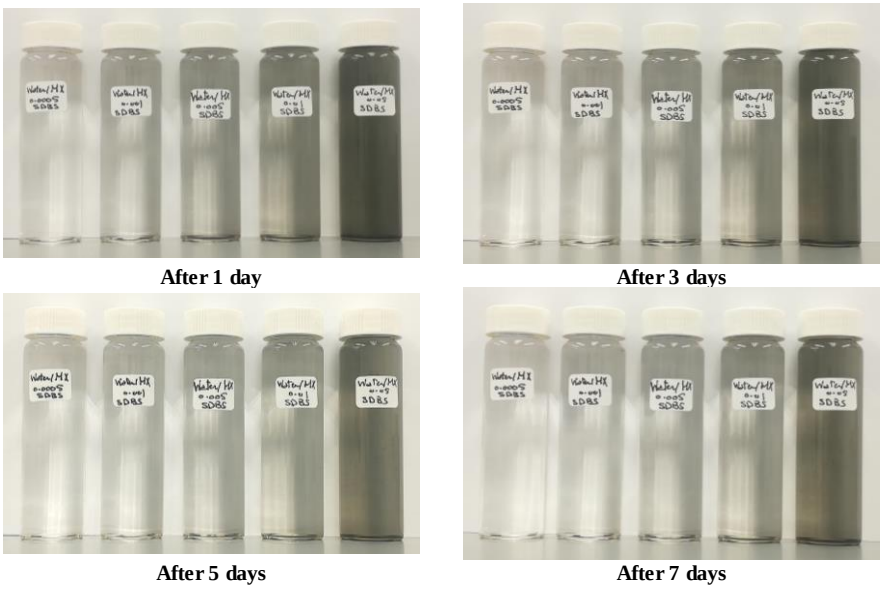

Figure 5 Visual observation to determine the stability of water/MXene samples prepared with the SDBS surfactant during 7 days after preparation

3.1.3 Monitoring of transmittance to assess the degradation of nanofluids

Monitoring the changes of the transmittance of the prepared nanofluid samples is another way to assess their stability. The transmittance spectra was measured daily for seven days in the range of 300 - 800 nm. Figure 6 demonstrates the variation of the transmittance spectra of the prepared nanofluids with a concentration of 0.05 wt. % using SDBS and CTAB, with time. The results indicate a noticeable increase in the transmittance of the samples after one day, indicating high sedimentation. The results seem to indicate that the change in transmittance is higher in the case of water/MXene nanofluid prepared using the SDBS surfactant compared to that prepared using the CTAB surfactant. However, by calculating the percentage increase in the overall transmittance with time by integrating the area under the spectral transmittance curves in Figure 6, a clearer picture is obtained as depicted in Figure 7. The results in Figure 7 for the three concentrations of 0.0005 wt. %, 0.005 wt. %, and 0.05 wt. % indicate that CTAB results in more stable water/MXene nanofluids at 0.05 wt. %, while the SDBS surfactant produces more stable nanofluids at lower MXene concentrations.

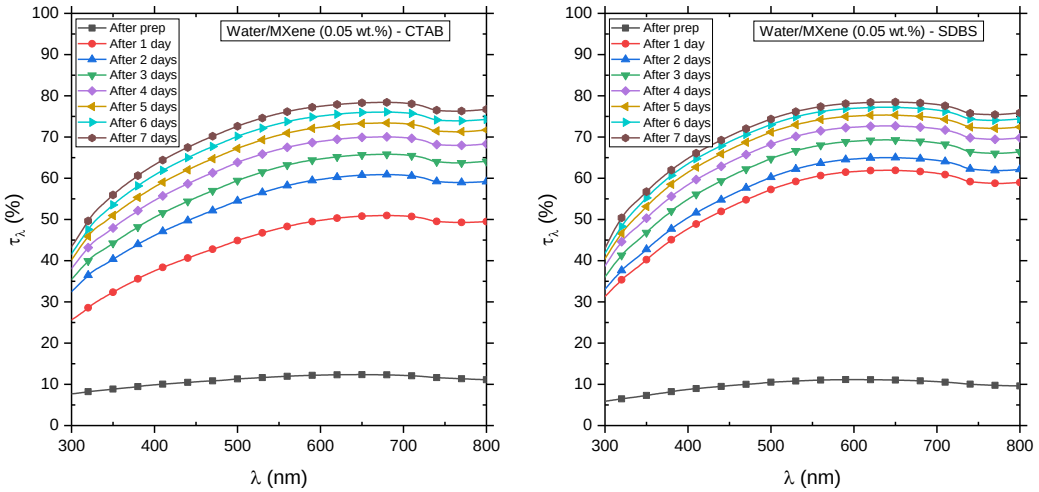

387

388 **Figure 6 Increase of the spectral transmittance with time indicating the degradation of the of the 0.05 wt. % water/MXene**
389 **nanofluid samples prepared using either CTAB or SDBS surfactant.**

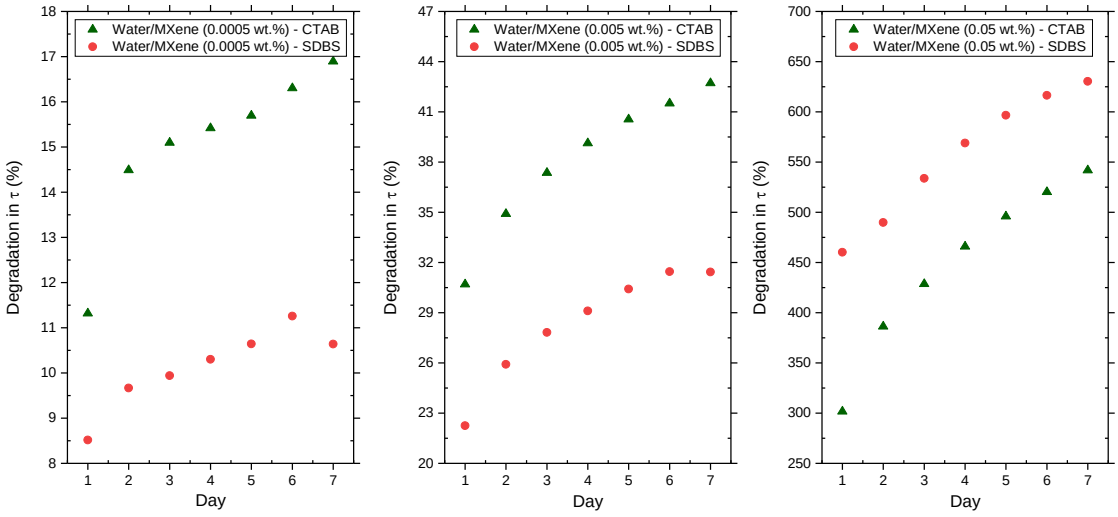

390

391 **Figure 7 The percentage increase in the transmittance of the water/MXene nanofluid samples of 0.0005 wt. %, 0.005 wt. %, and**
392 **0.05 wt. % prepared using either CTAB or SDBS surfactant.**

393 ## 3.2 Morphology of the water/MXene nanofluids

394 FESEM images of the synthesized MXene (Ti_3C_2) nanoflakes are illustrated in Figure 8 (a) and (b),
395 which indicate the structures have been exposed, revealing the individual sheets of the MXene along the
396 basal planes. The chemical etching process successfully exfoliates the MXene layers and the resulted
397 sheets display accordion-like topography. This finding is well correlated with the morphology of the
398 MXene synthesized by using the same MAX phase of Ti_3AlC_2 in a past work [18]. Energy dispersive
399 spectroscopic (EDS) analysis confirms the presence of Ti, C, O, F, and Cl elements without any trace
400 element of Al. The absence of Al indicates its complete elimination, which the Al-C layers have been

chemically removed from the structure of precursor material, transforming the MAX phase to the Mxene [18].

Figure 8(c) and (d) depict the SEM images of the 0.05 wt. % MXene nanofluidsin the presence of surfactants CTAB and SDBS, respectively. The images indicate that the surfactants assist the dispersion of MXene nanoflakes in water. The molecules of surfactant are most likely attach on the basal planes and in-between the layers of MXene [30,31], which enhance the dispersibility of MXene in water [31].

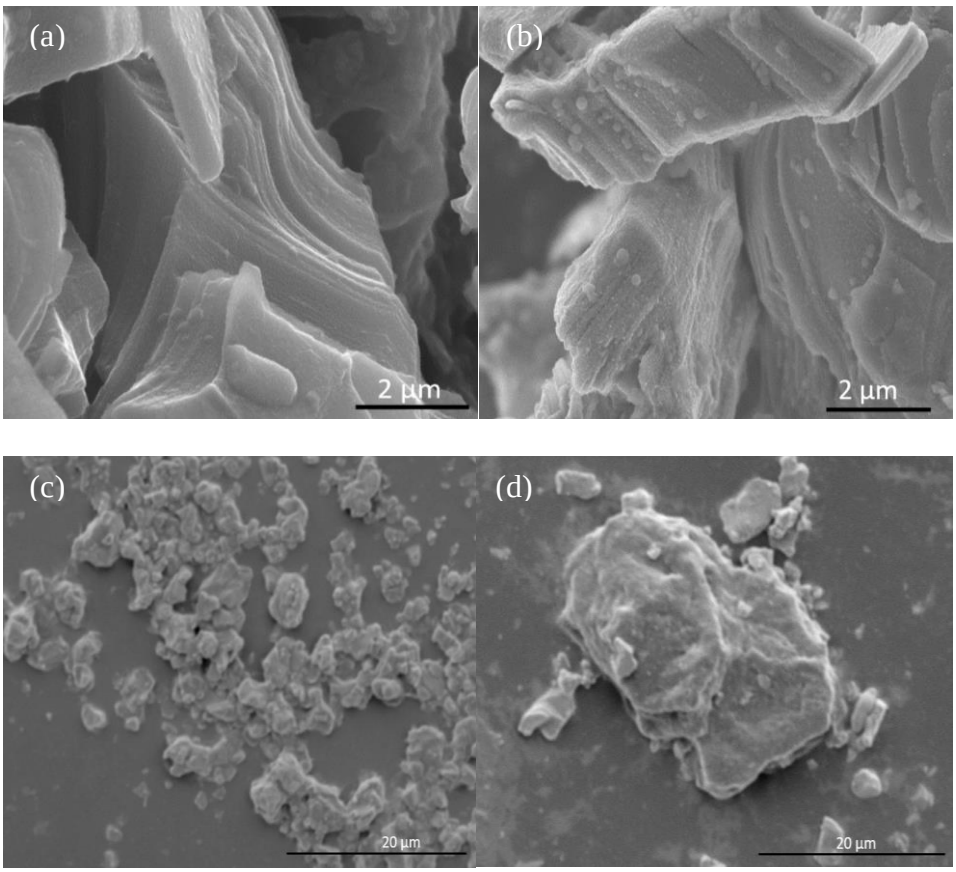

Figure 8 FESEM images of the MXene synthesized by using the mixture of LiF and HCl solution treatment. (a) Cross-sectional view and (b) top view; SEM images of 0.05 wt. % MXene nanofluids with the surfactants of (c) CTAB and (d) SDBS.

3.3 Fourier transform infrared (FTIR) spectroscopy

The FTIR spectra of deionized water and the water/MXene nanofluid samples with different concentrations of MXene have been conducted in the range of 4000-1000 cm^{-1}, as shown in Figure 9. All nanofluid samples prepared using different surfactants at all concentrations display identical spectra to that of the deionized water. The absorption peaks of all samples are at 3321 cm^{-1} and 1644 cm^{-1}. The results indicate that the interaction between the MXene nanoparticles and the deionized water facilitated by the surfactants CTAB or the SDBS is only physical and not chemical. These results are confirmed

by those previously reported by Kotia et al. [32], who observed identical peaks for the nanofluids and the base fluid.

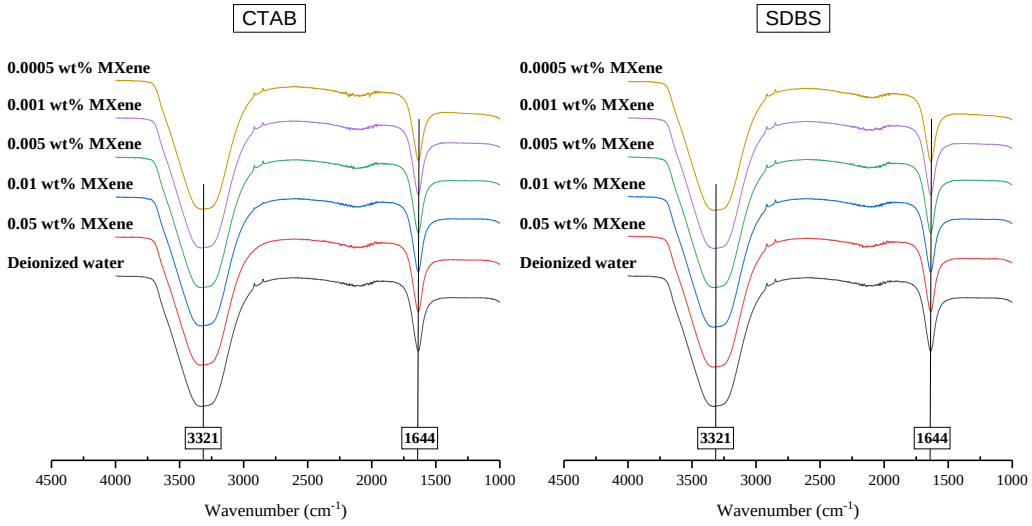

Figure 9 FTIR spectra of deionized water and water/MXene nanofluids prepared using surfactants CTAB and SDBS at concentrations of 0.0005, 0.001, 0.005, 0.01, and 0.05 wt. % in the range of 4000-1000 cm-1.

3.4 Optical properties of the water/MXene (Ti_3C_2)

Figure 10(a) and (b) illustrate the influence of the MXene nanoflakes concentration, on the transmittance spectra of the prepared water/MXene nanofluids by using the two surfactants CTAB and SDBS. The spectral transmittance curves were plotted using the measurements of the UV-Vis spectrophotometer. For both surfactants, an inverse relationship was observed between the MXene nanoflakes concentration and the transmittance spectra of the prepared water/MXene samples. The influence of the nanoflakes concentration on the transmittance spectra was significant. The effect of the surfactant and the nanoparticles-concentration was most observed in the range of 300 – 1350 nm, which corresponds to the Ultraviolet (UV), the Visual (Vis) and the Near Infrared (NIR) ranges. In contrary, the effect was negligible at higher wavelengths, which correspond to the Mid Infrared (MIR) range. With the CTAB surfactant (Figure 10 (a)), the rate of the reduction in the transmittance spectra with increasing concentration is low at lower concentrations (0.0005 wt. %, 0.001 wt. %, and 0.005 wt. %) and the transmittance decreases mainly in the range of 300-900 nm. A relatively smaller decrease in the transmittance spectra was observed in between 900 nm and 1350 nm. At higher MXene concentrations of 0.01 wt. % and 0.05 wt. %, a much more significant reduction in the transmittance is observed in the range of 300-1350 nm. The transmittance spectra of the water/MXene nanofluid samples prepared using CTAB with the concentrations of 0.001, 0.005, 0.01, and 0.05 wt. % at 700 nm are decreased by 6.7, 16.1, 44.4, and 86.6%, respectively, with respect to that of 0.0005 wt. % nanofluid sample. Only about

10% of radiation is transmitted by the studied nanofluids when the concentration of the nanoparticles is 0.05 wt. %.

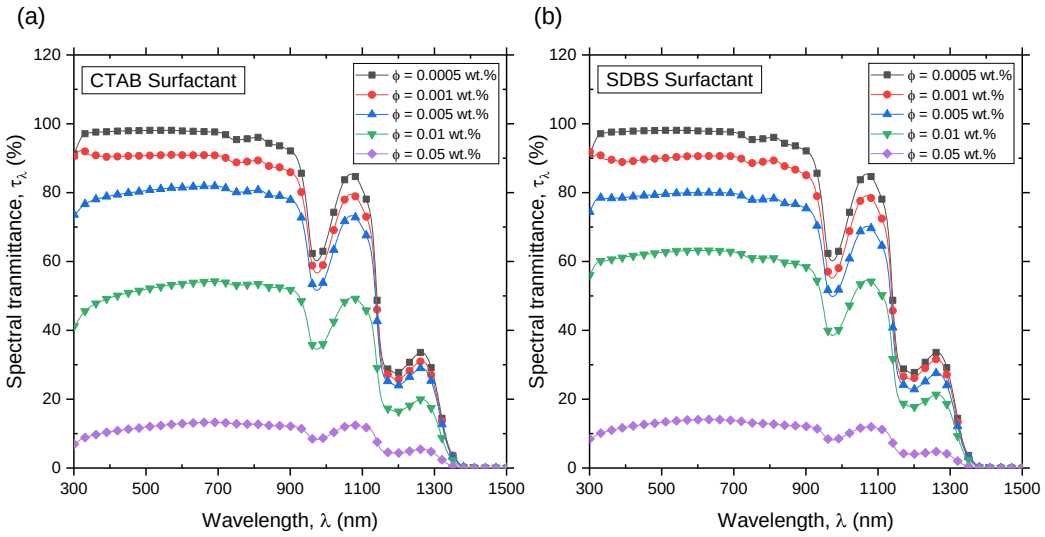

Figure 10 Transmittance spectra of the water/MXene nanofluid at different concentrations of nanoflakes prepared using: (a) CTAB surfactant, (b) SDBS surfactant

The variation of the transmittance spectra of the prepared water/MXene samples as a function of different concentrations of the nanoparticles by using SDBS is similar to that of the samples prepared using CTAB (Figure 10 (b)). However, the decrease of the transmittance of the sample with 0.05 wt. % of nanoparticles with reference to that with 0.01 wt. % is larger when compared to that observed with samples prepared using CTAB. The results indicate that the surfactant type has an influence on the transmittance spectra of the final nanofluid product. The water/MXene nanofluid samples prepared using the SDBS surfactant display a higher spectral transmittance when compared to those prepared using the CTAB surfactant, as the comparison for 0.01 wt. % samples depicted in Figure 11 indicates.

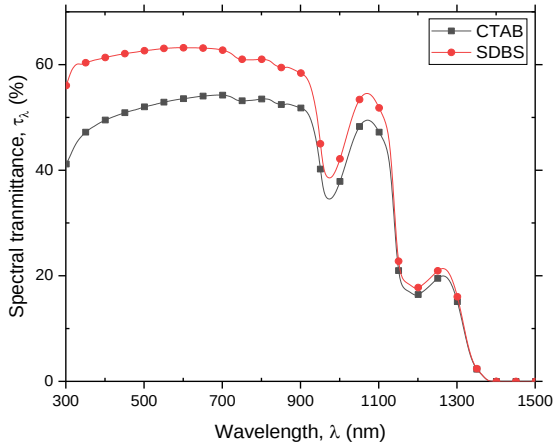

Figure 11 Comparison between the transmittance spectra of the water/MXene nanofluid samples of 0.01 wt. % prepared using CTAB and SDBS surfactants.

The transmittance spectra of the water/MXene nanofluid at different MXene nanoflakes concentrations prepared by using CTAB and SDBS was compared to verify the effect of the surfactants. Results of the comparison shown in Figure 12 indicate that, in most cases, using the SDBS surfactant is better than using CTAB, as SDBS does not significantly affect the transmittance of the original nanofluid in comparison to the CTAB.

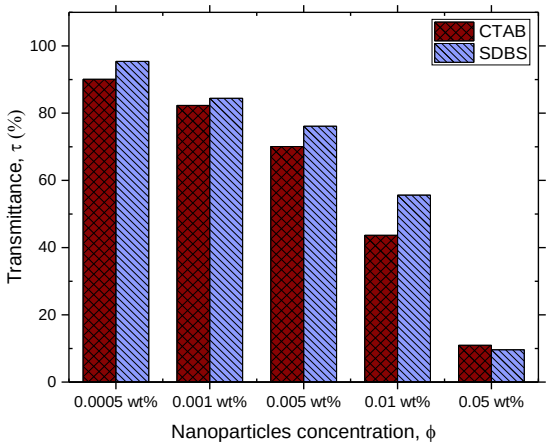

Figure 12 Comparison of the transmittance spectra of water/MXene nanofluid samples at different MXene-nanoparticles concentrations, prepared using CTAB and SDBS surfactants.

Absorbance (*A*) of all samples increases gradually with the decreasing wavelength in the range 280-800 nm (Figure 13). Even the nanofluids with the lowest concentration of MXene (0.0005 wt. %) prepared using both surfactants display a detectable absorbance [21,33,34]. A broad absorption band is observed within the visible range of 400-800nm, which becomes distinct with increasing concentration of MXene. This absorption band is attributed to the surface plasmon resonance (SPR) effect of MXenes [20,35,36]. All these findings indicate that MXenes in aqueous solution are capable of absorbing light at both UV and visible wavelengths. MXenes have been applied as photo-thermal materials instead of CNTs and reduced graphene oxide materials [20,33,37]. The MXene nanofluids prepared with SDBS display a higher *A* in the entire wavelength range, as compared to the MXene nanofluids prepared using CTAB. The light absorption capability of MXenes in the presence of SDBS is relatively better than that in the presence of CTAB. As the absorbance can be used as an indicator of the quality of dispersion of an absorbing species [38,39], the results indicate that MXene disperses better in the presence of SDBS, as evidenced by the previous results that display the better stability of the water/MXene nanofluids prepared by using the SDBS surfactant (Figure 7).

All samples display the maximum absorption peaks in the same range of 280-288 nm, which are due to theπ-π* transition of the C=C bond and n-π* transition of the C=O bond. These transitions typically

occur in the 250-300 nm range in carbon nanostructures, such as graphene nanosheets, quantum nanodots, or nanoparticles [22,35,40,41]. The SPR of the free π electron cloud of carbonaceous material also contributes to this absorption [42]. The intensity of these SPR peaks is proportional to the amount of MXenes when they contain carbon. That is why *A* increases with increasing concentration of MXenes and they disperse well in aqueous solutions.

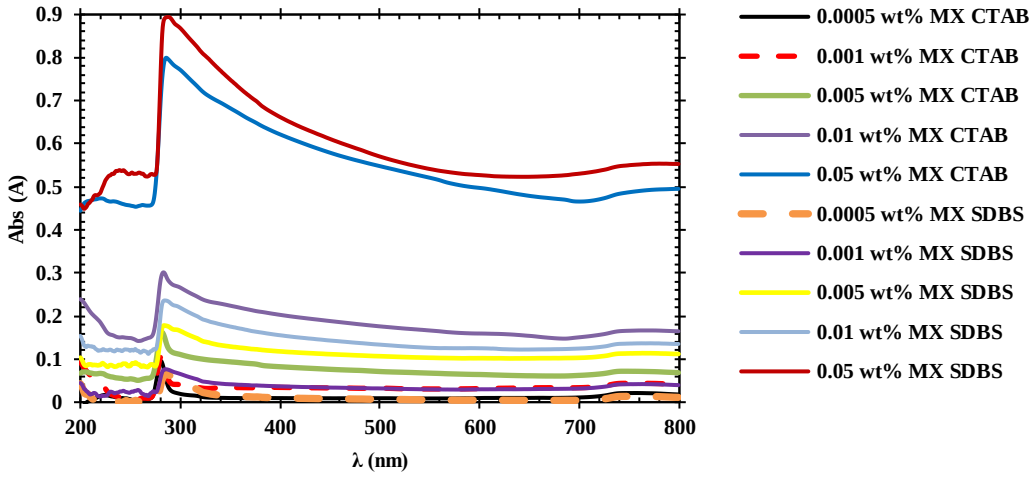

Figure 13 Absorption spectra of nanofluids with different concentrations of MXenes prepared using 0.36 mM CTAB and 0.38 mM SDBS.

The maximum absorption peaks of water/MXene (0.05 wt. %) prepared with both CTAB and SDBS occur at 286 nm (Figure 13). The plots of the absorbance at 286 nm versus the concentration of the water/MXene nanofluids are linear, as presented in Figure 14, indicating that the nanofluids obey the Beer-Lambert law [20,21]. The best fit of the two plots based on linear regression has coefficients of determination (R^2) close to 1.

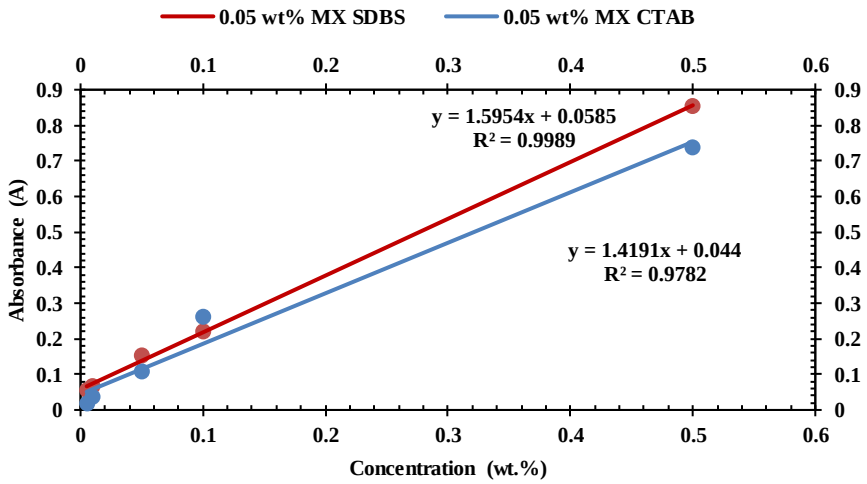

Figure 14 Absorbance as a function of concentration of MXenes prepared using CTAB and SDBS at a fixed wavelength of 286 nm.

The results indicate that A is directly proportional to the concentration (c) of MXenes measured with a light path length of 1cm. The molar absorptivity, ε_A, which is a measure of how strong MXenes absorbs light at a given wavelength per unit concentration [21], is calculated using Eq. 1. The calculated ε_A at 286 nm is about 1.4 $Lg^{-1}cm^{-1}$ and 1.6 $Lg^{-1}cm^{-1}$ for CTAB and SDBS, respectively. Light is adequately absorbed by the solutions in the presence of MXenes. With a higher value of ε_A, only a small concentration of MXenes is required to provide sufficient light absorption capability, which is ideal for the needs of nanofluid applications [43]. However, the ε_A calculated in this study differs from literature value, which has been determined at a wavelength of about 800 nm [20,35,44]. Nanoparticles of different size and different surface functional groups on MXenes resulting from different etching reagents and intercalants can cause variations of ε_A. Both LiF and HCl have been used as etching reagents, while Li^+ cations are used as intercalants to delaminate MXenes in this study [35]. The nature of the medium surrounding the nanoparticles also strongly influences ε_A [39]. The MXene nanofluids prepared using SDBS display a higher value of ε_A, which explains why MXene disperses better in the presence of SDBS and provides better absorption, as compared to the nanofluids containing CTAB, which confirms the results described earlier in the section describing the stability of the nanofluids.

The nanofluids with the highest concentration of MXene (0.05 wt. %) prepared using CTAB and SDBS have the best dispersion of nanoparticles, as evidenced by their highest values of A (Figure 13). Hence, both these samples are further studied to evaluate their absorption coefficient α using Eq. 3. The two nanofluids display similar behaviour and α gradually increases with the photon energy (E), then decreases starting in the range of 4.3-4.5 eV in both cases (Figure 15). When the light absorbed by an absorbing species (i.e., MXene) increases with increasing photon energy, αalso increases. Although α decreases drastically at about 4.3 eV, it still remains above $1cm^{-1}$ in the wavelength range of 200-800nm, unlike the carbon nanostructures, such as graphene or carbon nanoparticles for which α decreases to zero when the photon energy is higher than 4.3eV [22]. The maximum peaks in both samples are due to the characteristic SPR effect [22,38]. The behaviour of α is similar to that of ε_A described earlier, and α of MXene nanofluids prepared using SDBS is higher than that of the nanofluids prepared using CTAB. In the nanofluids with the highest concentration of MXenes, the nanoparticles disperse slightly better in the presence of SDBS, which is indicated by the higher A in the entire wavelength range resulting in a higher α overall.

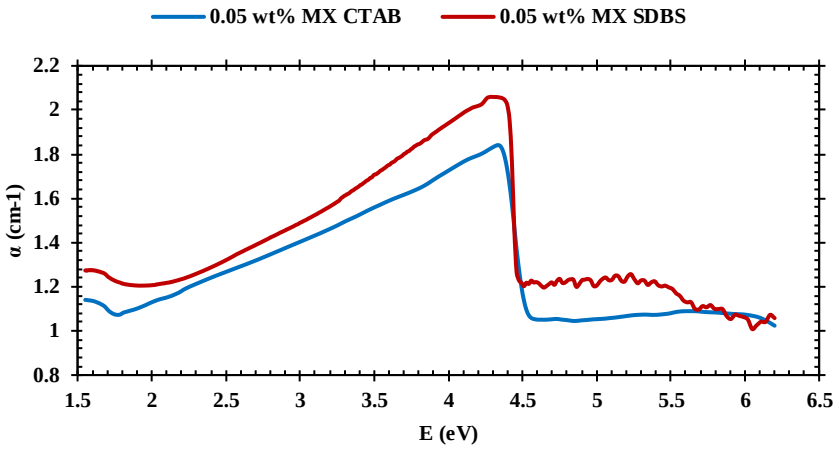

Figure 15 Absorption coefficient (α) as a function of photon energy (E) between of water/MXene nanofluids prepared using in CTAB and SDBS.

Band gap of a material is an important criterion in the semiconductor and nanomaterial industries. Insulators have a larger band gap (> 4eV) than semiconductors (< 3eV). To the best of our knowledge, there are a very limited number of experimental studies undertaken to investigate the band gap of MXenes. Based on the literature, the available reference values for these 2D materials are predicted by applying HSE06 hybrid density functionals [35]. In this study, the band gap energy of the nanofluids with the highest concentration of 0.05 wt. % MXenes dispersed using CTAB or SDBS are determined using the Tauc method employing the Kubelka-Munk function described by Eq. 6 [24–26].

The Tauc plots of the water/MXene nanofluids prepared using SDBS and CTAB are presented in Figure 16 for n=1/2, which corresponds to a direct allowed transition in MXene [22]. The values of E_g determined from the Tauc plots are 3.1 eV and 2.8 eV for water/MXene nanofluids prepared using CTAB and in SDBS, respectively, indicating that they behave as semiconductors due to surface functionalization [45]. During the etching process of Al-containing MAX phases, Al is selectively etched away and replaced by O, OH, or F surface terminations due to the use of both LiF and HCl as the etching reagents. They are then bonded to the Ti layers to form MXenes. When more of the metal surface has above terminations, the Fermi level of the metal is shifted lower and its density of state (DOS) at the Fermi level is reduced, resulting in a substantial band gap value [45–47]. Even though the E_g values determined in this study are smaller than that found in previous experimental work, it is still higher than that predicted by the computational method [35]. The variation of the band gap maybe due to the differences in the extent of surface functionalization, which cannot be easily controlled during synthesis. The surface of the MXenes is highly sensitive to the etching condition, which leads to the differences in their surface chemistry.

Better dispersion of MXene in the presence of SDBS as compared to CTAB is signalled by the higher values of A, ε_A, and α, resulting in the aforementioned results, which lowers E_g. Good dispersion of

MXene in aqueous solutions in the presence of SDBS further enhances the surface functionalization of the transition metal, which is mainly due to OH-termination rather than O- and F-terminations. The presence of OH-terminations reduces the high work function of the metal as compared to the O- and F-terminations, which results in a lower E_g [48]. In addition, OH-terminations are highly stable an environment with SDBS. Electrons are relatively easily excited from the valence and conduction bands when the band gap is low.

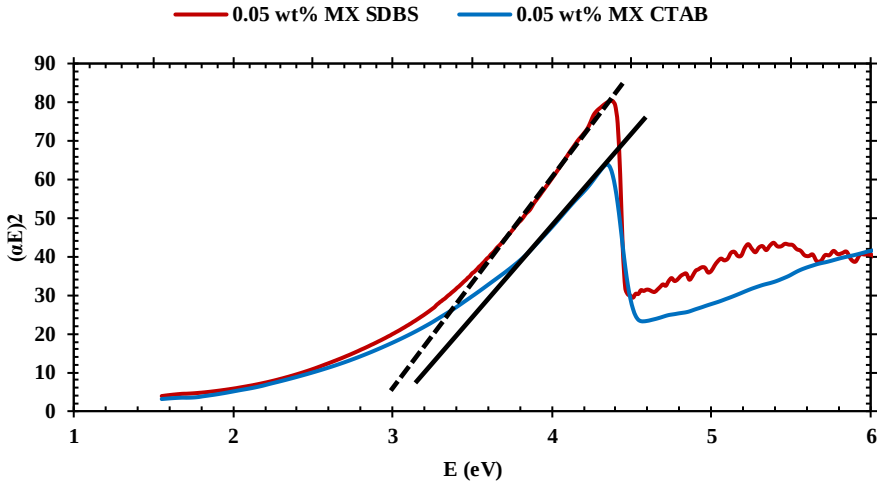

Figure 16 Tauc plot of0.05 wt. % water/MXene prepared using CTAB and SDBS.

3.5 Application for hybrid photovoltaic/thermal (PV/T) systems

By using the MXene in different concentrations (0.0005, 0.005, and 0.05 wt. %) as the optical filtration in the presence of two different surfactants (CTAB and SDBS), the performance of a hybrid PV/T system is investigated and compared to a conventional PV/T system without optical filtration. The comparisons in terms of the equivalent electrical efficiency and the temperature distribution along the PV panel are depicted in Figure 17. The results in Figure 19 (a) declare that the equivalent performance of the hybrid PV/T system with the water/MXene nanofluid at low MXene concentrations (0.0005 wt. %) is better than the conventional PV/T system without optical filtration. At MXene concentrations of 0.005 wt. %, the hybrid system with optical filtration starts to show lower equivalent performance compared to the conventional PV/T system and it reaches its lowest performance at concentration of 0.05 wt. %, due to the high obstruction of solar radiation. The equivalent electrical efficiency decreases with increasing concentration, most likely due to the increase of the absorptivity of the water/MXene nanofluid at high nanoparticles concentration, resulting in an enhancement in the thermal output and a reduction in the electrical output. The mid-day temperature distributions along the PV panel, depicted in Figure 17 (b) show lower temperatures accompanied with the addition of the optical filtration channel, which is attributed to the front-side cooling and attenuation of a part from the solar radiation to arrive at

the PV surface.

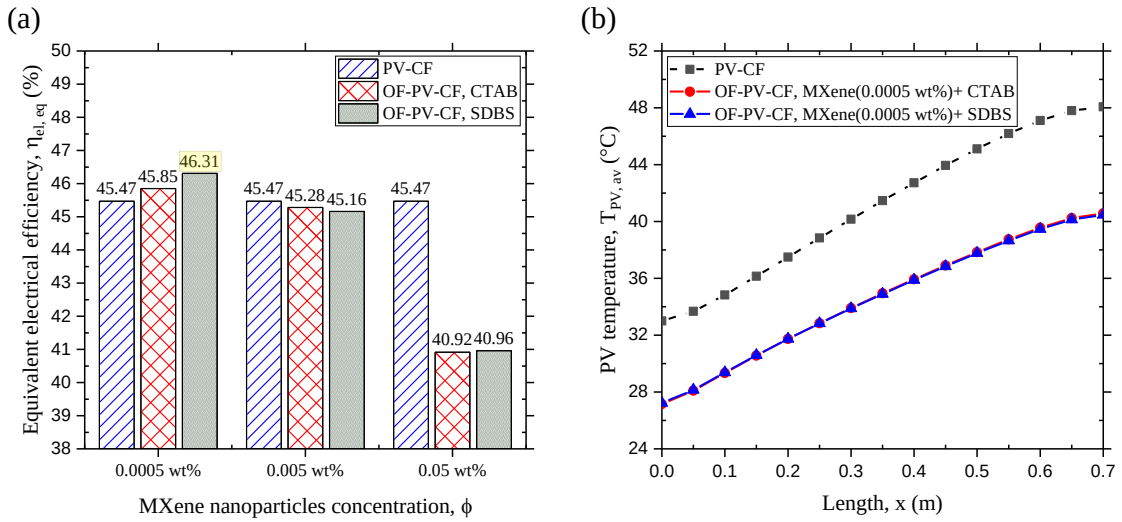

Figure 17 The equivalent electrical efficiency and the temperature distribution along the PV panel (at 12:00 pm) of the hybrid PV/T system with the water/MXene optical filtration at different concentrations of MXene nanoparticles, prepared with the use of either the CTAB or the SDBS surfactants in comparison to the conventional PV/T system without optical filtration

A breakdown of the output energies and efficiencies of the hybrid PV/T system with optical filtration provides a clearer picture of the impact of the concentration of the nanoparticles and the surfactant type, as illustrated in Figure 18 and Figure 19. The results indicate that increasing the concentration of the nanoparticles affects the electrical performance negatively by decreasing the electrical energy output (Figure 18 (a) and Figure 19 (a)), while it affects the thermal performance positively by increasing the thermal energy output (Figure 18 (b) and Figure 19 (b)). When optical filtration is used, a lower amount of solar radiation reaches the PV panel resulting in a lower electrical energy output in comparison to the conventional PV/T system without optical filtration. The ideal case of optical filtration is when the nanofluid allows full transmittance of solar radiation in the useful range for PV (325 – 1125 nm), which will not reduce the electrical energy output from the PV/T system (The reference efficiency of the panel in Figure 3). However, the water/MXene nanofluids used in this study are not able to achieve that. In addition, neglecting the change of the thermal conductivity of the water/MXene nanofluid samples with increasing concentration of the nanoparticles is another reason for the reduction of the electrical energy. As the thermal conductivity of a nanofluid with increasing concentration of nanoparticles is also expected to increase resulting in better cooling of the PV, a higher electrical energy output is anticipated. Many other parameters, such as the water/MXene mass flow rate and the channel height, can also affect the electrical energy.

Finally, a comparison of the results in Figure 17, Figure 18 and Figure 19 indicate that the SDBS surfactant shows better effect compared to the CTAB, when added to low concentrations from the MXene nanoparticles (0.0005 wt. %). At higher concentrations, both surfactants produce a very similar effect. Overall, the SDBS surfactant is slightly better, especially at lower concentrations, due to the

higher stability of the nanofluids it forms.

In conclusion, the use of a water/MXene nanofluid, at low nanoparticles concentrations, as the optical filtration in a hybrid PV/T system performs better than the conventional PV/T system without optical filtration. However, when the amount of MXene as optical filtration is 0.005 wt. % or above in hybrid PV/T system, the performance of the conventional PV/T system without optical filtration is better. More intense research should be conducted to investigate the effect of the mass flow rate of the nanofluid and the channel height on both the electrical and thermal performance of the hybrid PV/T system accompanied with optical filtration. The nanoparticles' size and shape as well as the types of surfactant are the important parameters to be optimized for getting the reliable efficiency in the hybrid PV/T system.

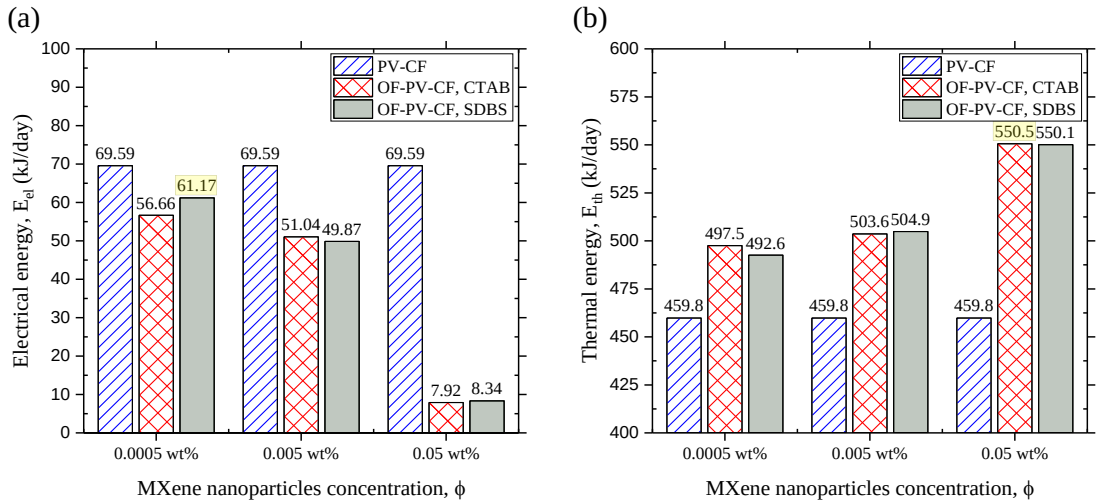

Figure 18 The electrical and thermal energies output from the hybrid PV/T system with the water/MXene optical filtration at different concentrations of MXene nanoparticles, prepared with either the use of the CTAB and the SDBS surfactants in comparison to the conventional PV/T system without optical filtration

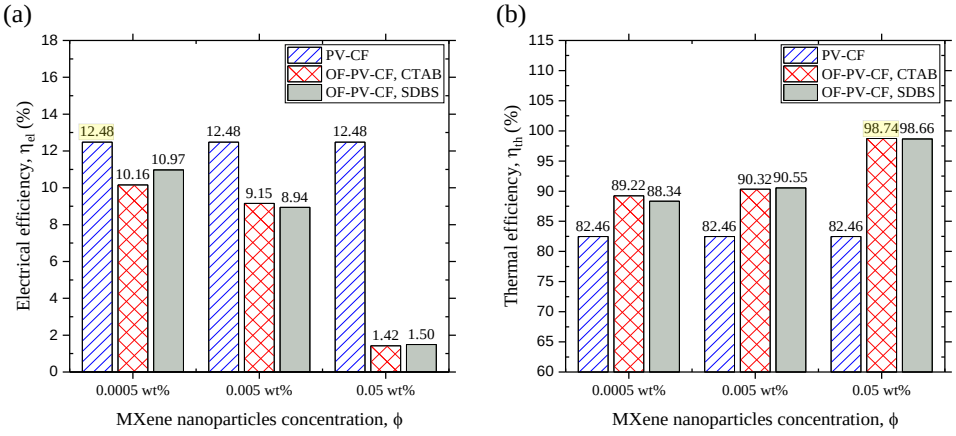

Figure 19 The electrical and thermal efficiencies of the hybrid PV/T system with the water/MXene optical filtration at different concentrations MXene nanoparticles, prepared with the use of either the CTAB or the SDBS surfactants in comparison to the conventional PV/T system without optical filtration

4. Conclusions

The effects of the concentration of MXene (Ti_3C_2) nanoflakes and the surfactants of CTAB and SDBS on the optical properties of the water/MXene nanofluids are evaluated. The dispersion stability of the water/MXene nanofluids is determined through visual inspection and by monitoring the transmittance change with time. The stability assessment conclusions are summarized as:

- Observation from visual inspection showed high degradation of the nanofluids at all concentrations after five days.
- Monitoring of transmittance change indicated that the nanofluid samples prepared using the CTAB surfactant are more stable at higher concentration of the nanoflakes. However, at lower concentration of the nanoflakes, the samples prepared using the SDBS surfactant were more stable.

For the findings of the UV-Vis spectroscopy:

- The nanoflakes concentration has a significant impact on the transmittance spectra.
- The transmittance decreases when the amount of nanoflakes increases.
- The effects of the type of surfactant and the concentration of the nanoflakes are most noticeable in the range of 300 - 1350 nm (the UV, Vis and NIR ranges).
- The water/MXene nanofluids prepared using the SDBS surfactant display a higher transmittance in comparison to those prepared using the CTAB surfactant.
- The SDBS surfactant affects the transmittance in a lesser extent, implying that it renders the nanofluid more stability. The MXene nanoflakes within an aqueous solution are capable of absorbing light in both the UV and visible wavelengths.

Implementing the measured optical properties in a hybrid PV/T system with an optical filtration facility declared a higher performance compared to the conventional PV/T system when the water/MXene nanofluid with a low concentration is used. At MXene concentrations above 0.05 wt. %, the hybrid system with optical filtration becomes electrically-inefficient.

5. Acknowledgements

R. Saidur would like to acknowledge the financial support provided by Sunway University, Malaysia, through the project No. STR-RCTR-RCNMET-001-2019. In addition, the authors appreciate the financial support provided by King Fahd University of Petroleum & Minerals(KFUPM), Saudi Arabia, through the project no. DSR-IN161059.

6. References

[1] Kuang Y, Zhang Y, Zhou B, Li C, Cao Y, Li L, et al. A review of renewable energy utilization in islands. Renew Sustain Energy Rev 2016;59:504–13. doi:10.1016/j.rser.2016.01.014.

[2] Xu Z. Optical Properties of Metal Clusters. J Am Chem Soc 1996;118:6098–6098. doi:10.1021/ja955378p.

[3] Justo JJ, Mwasilu F, Lee J, Jung JW. AC-microgrids versus DC-microgrids with distributed energy resources: A review. Renew Sustain Energy Rev 2013;24:387–405. doi:10.1016/j.rser.2013.03.067.

[4] Quoilin S, Broek M Van Den, Declaye S, Dewallef P, Lemort V. Techno-economic survey of organic rankine cycle (ORC) systems. Renew Sustain Energy Rev 2013;22:168–86. doi:10.1016/j.rser.2013.01.028.

[5] Gorji TB, Ranjbar AA. A review on optical properties and application of nanofluids in direct absorption solar collectors (DASCs). Renew Sustain Energy Rev 2017;72:10–32. doi:10.1016/j.rser.2017.01.015.

[6] Foley T, Thornton K, Hinrichs-rahlwes R, Sawyer S, Sander M, Taylor R, et al. Renewables 2015 global status report. vol. 4. 1988. doi:10.1016/0267-3649(88)90030-1.

[7] Phelan P, Otanicar T, Taylor R, Tyagi H. Trends and opportunities in direct-absorption solar thermal collectors. J Therm Sci Eng Appl 2013;5. doi:10.1115/1.4023930.

[8] Minardi JE, Chuang HN. Performance of a “black” liquid flat-plate solar collector. Sol Energy 1975;17:179–83. doi:10.1016/0038-092X(75)90057-2.

[9] Mu, L., Q. Zhu, and L. Si. Radiative properties of nanofluids and performance of a direct solar absorber using nanofluids. in ASME 2009 second international conference on micro/nanoscale heat and mass transfer. 2010. American Society of Mechanical Enginee n.d.

[10] Sani E, Barison S, Pagura C, Mercatelli L, Sansoni P, Fontani D, et al. Carbon nanohorns-based nanofluids as direct sunlight absorbers. Opt Express 2010;18:5179. doi:10.1364/oe.18.005179.

[11] Mercatelli L, Sani E, Zaccanti G, Martelli F, Ninni P Di, Barison S, et al. Absorption and scattering properties of carbon nanohorn-based nanofluids for direct sunlight absorbers. Nanoscale Res Lett 2011;6:1–9. doi:10.1186/1556-276X-6-282.

[12] Taylor R a, Phelan PE, Otanicar TP, Adrian R, Prasher R. Nanofluid optical property characterization: towards efficient direct absorption solar collectors. Nanoscale Res Lett 2011;6:225. doi:10.1186/1556-276X-6-225.

[13] Said Z, Sajid MH, Saidur R, Mahdiraji GA, Rahim NA. Evaluating the Optical Properties of TiO2 Nanofluid for a Direct Absorption Solar Collector. Numer Heat Transf Part A Appl

2015;67:1010–27. doi:10.1080/10407782.2014.955344.

[14] Tyagi H, Phelan P, Prasher R. Predicted Efficiency of a Low-Temperature Nanofluid-Based Direct Absorption Solar Collector. J Sol Energy Eng 2009;131:041004. doi:10.1115/1.3197562.

[15] Jing D, Hu Y, Liu M, Wei J, Guo L. Preparation of highly dispersed nanofluid and CFD study of its utilization in a concentrating PV/T system. Sol Energy 2015;112:30–40. doi:10.1016/j.solener.2014.11.008.

[16] Lee BJ, Park K, Walsh T, Xu L. Radiative heat transfer analysis in plasmonic nanofluids for direct solar thermal absorption. J Sol Energy Eng Trans ASME 2012;134. doi:10.1115/1.4005756.

[17] Taylor RA, Otanicar T, Rosengarten G. Nanofluid-based optical filter optimization for PV/T systems. Light Sci Appl 2012;1:1–7. doi:10.1038/lsa.2012.34.

[18] Naguib M, Kurtoglu M, Presser V, Lu J, Niu J, Heon M, et al. Two-dimensional nanocrystals produced by exfoliation of Ti 3AlC 2. Adv Mater 2011;23:4248–53. doi:10.1002/adma.201102306.

[19] Shahzad F, Alhabeb M, Hatter CB, Anasori B, Hong SM, Koo CM, et al. Electromagnetic interference shielding with 2D transition metal carbides (MXenes). Science (80-) 2016;353:1137–40. doi:10.1126/science.aag2421.

[20] Li R, Zhang L, Shi L, Wang P. MXene Ti3C2: An Effective 2D Light-to-Heat Conversion Material. ACS Nano 2017;11:3752–9. doi:10.1021/acsnano.6b08415.

[21] Wulandari D. Spectrophotometry Overview 2017.

[22] Sadeghi H, Dorranian D. Influence of size and morphology on the optical properties of carbon nanostructures. J Theor Appl Phys 2016;10:7–13. doi:10.1007/s40094-015-0194-4.

[23] Lee SH, Jang SP. Extinction coefficient of aqueous nanofluids containing multi-walled carbon nanotubes. Int J Heat Mass Transf 2013;67:930–5. doi:10.1016/j.ijheatmasstransfer.2013.08.094.

[24] Tauc, J., R. Grigorovici, and A.J.p.s.s. Vancu, Optical properties and electronic structure of amorphous germanium. 1966. 15(2): p. 627-637 n.d.

[25] Chen J, Tang W, Xin L, Shi Q. Band gap characterization and photoluminescence properties of SiC nanowires. Appl Phys A Mater Sci Process 2011;102:213–7. doi:10.1007/s00339-010-5943-2.

[26] El-Denglawey A, Dongol M, El-Nahass MM. Photoinduced absorption edge shift of As20Se60Tl20 films. J Lumin 2010;130:801–4. doi:10.1016/j.jlumin.2009.11.036.

[27] Weather Spark. https://weatherspark.com/y/104950/Average-Weather-in-Dhahran-Saudi-Arabia-Year-Round n.d.

[28] International standard ISO 9845-1, standard solar spectra ASTM G-173-03, <http://pveducation.org/pvcdrom/appendices/standard-solar-spectra> n.d.

[29] Wikipedia. https://en.wikipedia.org/wiki/Energy_conversion_efficiency n.d.

[30] Lotya M, Hernandez Y, King PJ, Smith RJ, Nicolosi V, Karlsson LS, et al. Liquid phase production of graphene by exfoliation of graphite in surfactant/water solutions. J Am Chem Soc 2009;131:3611–20. doi:10.1021/ja807449u.

[31] Vadukumpully S, Paul J, Valiyaveettil S. Cationic surfactant mediated exfoliation of graphite into graphene flakes. Carbon N Y 2009;47:3288–94. doi:10.1016/j.carbon.2009.07.049.

[32] Kotia A, Haldar A, Kumar R, Deval P, Ghosh SK. Effect of copper oxide nanoparticles on thermophysical properties of hydraulic oil-based nanolubricants. J Brazilian Soc Mech Sci Eng 2017. doi:10.1007/s40430-016-0664-x.

[33] Yu X, Cai X, Cui H, Lee SW, Yu XF, Liu B. Fluorine-free preparation of titanium carbide MXene quantum dots with high near-infrared photothermal performances for cancer therapy. Nanoscale 2017;9:17859–64. doi:10.1039/c7nr05997c.

[34] Mayerhöfer TG, Popp J. Beer's Law – Why Absorbance Depends (Almost) Linearly on Concentration. ChemPhysChem 2019;20:511–5. doi:10.1002/cphc.201801073.

[35] Hantanasirisakul K, Gogotsi Y. Electronic and Optical Properties of 2D Transition Metal Carbides and Nitrides (MXenes). Adv Mater 2018;30:0–30. doi:10.1002/adma.201804779.

[36] Chertopalov S, Mochalin VN. Environment-Sensitive Photoresponse of Spontaneously Partially Oxidized Ti3C2 MXene Thin Films. ACS Nano 2018;12:6109–16. doi:10.1021/acsnano.8b02379.

[37] Ling Z, Ren CE, Zhao MQ, Yang J, Giammarco JM, Qiu J, et al. Flexible and conductive MXene films and nanocomposites with high capacitance. Proc Natl Acad Sci U S A 2014;111:16676–81. doi:10.1073/pnas.1414215111.

[38] Yu J, Grossiord N, Koning CE, Loos J. Controlling the dispersion of multi-wall carbon nanotubes in aqueous surfactant solution. Carbon N Y 2007;45:618–23. doi:10.1016/j.carbon.2006.10.010.

[39] Njuguna J, Vanli OA, Liang R. A Review of Spectral Methods for Dispersion Characterization of Carbon Nanotubes in Aqueous Suspensions. J Spectrosc 2015;2015. doi:10.1155/2015/463156.

[40] Chen JL, Yan XP. A dehydration and stabilizer-free approach to production of stable water

dispersions of graphene nanosheets. J Mater Chem 2010;20:4328–32. doi:10.1039/c000177e.

[41] Kumar V, Singh V, Umrao S, Parashar V, Abraham S, Singh AK, et al. Facile, rapid and upscaled synthesis of green luminescent functional graphene quantum dots for bioimaging. RSC Adv 2014;4:21101–7. doi:10.1039/c4ra01735h.

[42] Ghanbari H, Sarraf-mamoory R, Sabbaghzadeh J, Chehrghani A. Nonlinear Optical Absorption of Carbon Nanostructures Synthesized by Laser Ablation of Highly Oriented Pyrolytic Graphite in Organic Solvents 2013;7:1–12.

[43] Khullar V, Bhalla V, Tyagi H. Potential heat transfer fluids (Nanofluids) for direct volumetric absorption-based solar thermal systems. J Therm Sci Eng Appl 2018;10. doi:10.1115/1.4036795.

[44] Xuan J, Wang Z, Chen Y, Liang D, Cheng L, Yang X, et al. Organic-Base-Driven Intercalation and Delamination for the Production of Functionalized Titanium Carbide Nanosheets with Superior Photothermal Therapeutic Performance. Angew Chemie - Int Ed 2016;55:14569–74. doi:10.1002/anie.201606643.

[45] Khazaei M, Ranjbar A, Arai M, Sasaki T, Yunoki S. Electronic properties and applications of MXenes: a theoretical review. J Mater Chem C 2017;5:2488–503. doi:10.1039/c7tc00140a.

[46] Khazaei M, Arai M, Sasaki T, Chung CY, Venkataramanan NS, Estili M, et al. Novel electronic and magnetic properties of two-dimensional transition metal carbides and nitrides. Adv Funct Mater 2013;23:2185–92. doi:10.1002/adfm.201202502.

[47] Sun W, Xie Y, Kent PRC. Double transition metal MXenes with wide band gaps and novel magnetic properties. Nanoscale 2018;10:11962–8. doi:10.1039/c8nr00513c.

[48] Khazaei M, Arai M, Sasaki T, Ranjbar A, Liang Y, Yunoki S. OH-terminated two-dimensional transition metal carbides and nitrides as ultralow work function materials. Phys Rev B - Condens Matter Mater Phys 2015;92:1–28. doi:10.1103/PhysRevB.92.075411.